Excitation of Guided Waves on a Lossless Dielectric Slab by an E-Polarized Complex Source Point Beam

Nikolaos L. Tsitsas, *Member, IEEE*, Constantinos Valagiannopoulos, *Senior Member, IEEE*, and Alexander I. Nosich, *Fellow, IEEE*

***Abstract*— A lossless slab excited by an E-polarized two-dimensional (2-D) complex source point (CSP) beam is studied analytically. Such a source, unlike a Gaussian beam, satisfies exactly the Helmholtz equation and radiation condition, without paraxial approximation or formulation incompleteness. The guided-waves fields as well as the scattered fields in the regions above and below the slab are determined; in turn, the corresponding powers are directly calculated. Numerical results on the variations of these quantities with respect to the slab electrical thickness, the beam angle of incidence, the source aperture size and location are presented. Substantial power transfer from the finite directive source into each of the slab's guided waves is recorded especially in the case of near-grazing beam illumination. Such a finding may inspire further theoretical and experimental efforts towards numerous research directions like non-invasive sensing, wireless optical tagging and energy teleportation.**

***Index Terms*— Complex beams, guided waves, scattering, slabs, waveguides.**

I. Introduction

TRANSMISSION and reflection of a directive wave beam by a dielectric slab has gained considerable attention in many applications in optics and microwaves. In most of the relevant publications, such a beam was assumed to be a Gaussian beam [1]–[5]. Although this has brought many useful results, it must be noted that using a Gaussian beam in wave scattering formulations is mathematically controversial because, unlike the scattered field, it is not a solution to the Helmholtz or Maxwell equations and does not satisfy the radiation condition at infinity. Additionally, Gaussian beam field magnitude is symmetric with respect to its waist section which is not the case for any realistic source such as small horn or lens antennas.

The alternative was proposed in [6]. This is a complex source point (CSP) beam, which is the exact solution of the Helmholtz or Maxwell equations and satisfies the radiation condition at infinity. Additionally, it has asymmetric wave field with maximum magnitude along only one direction, normal to its aperture. The power carried by a CSP beam is finite, similar to Gaussian beam but contrary to the plane wave power. Actually, the CSP beam asymptotically coincides with the Gaussian beam in the paraxial domain of the near-field zone. Thus, it can adequately model a directive feed placed at a finite distance from scatterers.

CSP beams were used as incident fields in flat-interface scattering [7], [8], and reflector and lens antennas [9]–[15], and as basis functions in numerical discretization in [16]–[19]. Recently, they were used in two-dimensional (2-D) photonic crystal scattering [20], wedge scattering [21], and for investigating absorption by a lossy grounded dielectric slab with a superstrate [22].

The case of a lossless dielectric slab is important in view of its ability to guide natural waves. The effect of the guided waves was completely neglected or overlooked in [1]–[5] where only the beam transmission and reflection was studied. Their excitation by a directive beam has much in common with the scattering of the same guided waves by inclusions and particles placed inside or near to the slab, studied in [23]–[31]. In particular, both types of problems need an adequate radiation condition at infinity as the Sommerfeld condition is no more valid, because of existence of nonattenuating guided waves. Such a modified condition was introduced in [25] (see also [32], [33]).

In this paper, we analytically study the electromagnetic scattering problem associated with the CSP excitation of a lossless dielectric slab and predict accurately the power captured by the guided waves and the power scattered to the outer space. More precisely, in Section II, we present the mathematical formulation of the scattering problem and the Fourier-integral expressions of the primary and secondary fields. In Section III, we explicitly determine the space wave far-field scattering

Manuscript received April 12, 2018; revised February 19, 2019; accepted April 15, 2019. Date of publication May 3, 2019; date of current version August 12, 2019. The work of C. Valagiannopoulos was supported by the Ministry of Education and Science of the Republic of Kazakhstan State-Targeted Program under Grant BR05236454, and in part by Nazarbayev University Faculty Development Competitive Research Grant through the Project "Super Transmitters, Radiators and Lenses via Photonic Synthetic Matter" under Grant 090118FD5349 and in part by Nazarbayev University ORAU Grant through the Project "Structured Light for Nonlinear and Topological Photonics" under Grant 20162031. *(Corresponding author: Nikolaos L. Tsitsas.)*

N. L. Tsitsas is with the School of Informatics, Aristotle University of Thessaloniki, 54124 Thessaloniki, Greece (e-mail: ntsitsas@csd.auth.gr).

C. Valagiannopoulos is with the Department of Physics, School of Science and Technology, Nazarbayev University, Astana 010000, Kazakhstan (e-mail: konstantinos.valagiannopoulos@nu.edu.kz).

A. I. Nosich is with the Laboratory of Micro and Nano Optics, Institute of Radio-Physics and Electronics, National Academy of Sciences of Ukraine (NASU), 61085 Kharkiv, Ukraine (e-mail: anosich@yahoo.com).

Color versions of one or more of the figures in this paper are available online at http://ieeexplore.ieee.org.

Digital Object Identifier 10.1109/TAP.2019.2913803

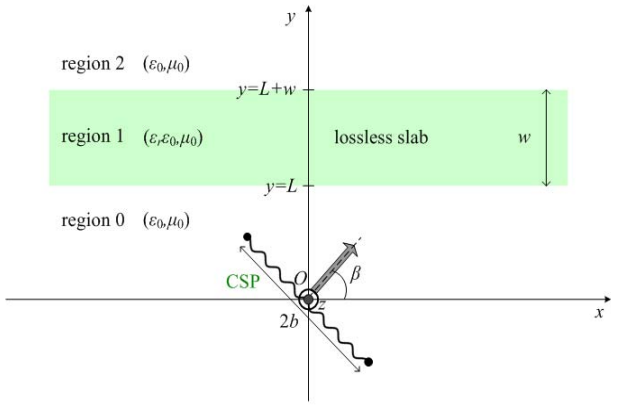

Fig. 1. Geometry and notations of the 2-D CSP beam illuminating a dielectric slab. The beam aperture is shown by a wavy line and has the width b and the orientation angle β.

patterns and the associated powers in the regions above and below the slab. Then, in Section IV, we derive the exact expressions of the fields of the guided waves propagating along the slab as well as their corresponding powers. In Section V, numerical results are presented concerning the variations of the guided-waves and scattered powers versus the parameters of the CSP beam and the slab. Numerical simulations by commercial software are also included, exhibiting the near-field features predicted by our full-wave analytical solution. Finally, Section VI contains concluding remarks and future work directions.

Some preliminary results of this analysis were reported in a conference paper [34]. This paper provides all details of derivations and presents additional and more convincing numerical results. An $\exp(\mathrm{i}\omega t)$ time dependence is assumed and suppressed throughout, with ω as the angular frequency, t as time, and $\mathrm{i} = \sqrt{-1}$.

II. Solution in the Fourier-Transform Domain

A lossless dielectric slab of thickness w and relative real dielectric permittivity ε_r is excited by a CSP beam (see Fig. 1) with its complex coordinates given by

$$\mathbf{r}_{CS} = (x_{CS}, y_{CS}) = \mathbf{r}_0 + \mathrm{i}\mathbf{b}, \quad \mathbf{r}_0 = (x_0, y_0), \quad \mathbf{b} = -b(\cos\beta, \sin\beta). \tag{1}$$

The real coordinates of the source are given by the vector $\mathbf{r}_0$, and we may consider, without loss of generality, that $(x_0, y_0) = (0, 0)$. The imaginary coordinates are given by the vector $\mathbf{b}$, and hence, by the real parameters b and β, which are, respectively, associated with the aperture width and the orientation angle of a horn antenna simulated by a CSP [5]–[10]. The distance between the center (0, 0) of the CSP aperture and the lower boundary of the slab is denoted by L. The lossless slab lies in vacuum with permittivity ε_0 and permeability μ_0. The entire configuration is uniform along the z-axis.

The z-component of the primary electric field, radiated by the CSP in the free space, is given by

$$E^{\mathrm{pr}}(\mathbf{r}, \mathbf{r}_{CS}) = -\frac{\mathrm{i}}{4} H_0^{(2)}(k_0|\mathbf{r} - \mathbf{r}_{CS}|) \tag{2}$$

where $H_0^{(2)}$ denotes the second-kind cylindrical Hankel function of the order 0, and $k_0 = \omega/c$ is the free-space wavenumber (c is the light velocity). For $b \neq 0$, (2) has two singular branch points at $(x_0 \pm b\sin\beta,\ y_0 \mp b\cos\beta)$. They call for introduction of a branch-cut in the plane of real-valued coordinates connecting the mentioned points, which can be viewed as endpoints of the CSP aperture (see Fig. 1).

Note that the field (2) is the exact solution of the Helmholtz equation with respect to the observation point $\mathbf{r}$

$$\left(\Delta_{\mathbf{r}} + k_0^2\right) E^{\mathrm{pr}}(\mathbf{r}; \mathbf{r}_{CS}) = -\delta(\mathbf{r} - \mathbf{r}_{CS}) \tag{3}$$

where δ is the delta function. It satisfies the 2-D Sommerfeld radiation condition at infinity and has a far-field pattern as follows:

$$E^{\mathrm{pr}}(\mathbf{r}, \mathbf{r}_{CS}) \sim \sqrt{2\pi/(k_0 r)}\, e^{-\mathrm{i}\left(k_0 r - \frac{\pi}{4}\right)} \Phi^{\mathrm{pr}}(\varphi), \quad r \to \infty \tag{4}$$

$$\Phi^{\mathrm{pr}}(\varphi) = -\left(\tfrac{\mathrm{i}}{4\pi}\right) e^{k_0 b\cos(\varphi+\beta)}, \quad 0 \le \varphi \le 2\pi \tag{5}$$

where $r = (x^2 + y^2)^{1/2}$ and $\tan\varphi = y/x$. Its beamwidth is controlled by $k_0 b$, as certified by the exponential factor in (5).

The primary CSP field is perturbed by the dielectric slab, thus generating the secondary field E^{sec} in all regions. The latter function satisfies the homogeneous Helmholtz equation with wavenumbers k_0 and $k_1 = k_0 \varepsilon_r^{1/2}$ in the vacuum and the slab, respectively, as well as the transmission boundary conditions at the slab's boundaries. As mentioned, the radiation condition for the secondary field has to be modified with respect to the free-space radiation condition due to the presence of guided waves in the lossless dielectric slab. Following [25], we demand that, far from the origin function, E^{sec} is the sum of an outgoing cylindrical wave off the slab domain and a finite sum of nonattenuating guided waves both inside and outside of that domain

$$E^{\mathrm{sec}}(\mathbf{r}, \mathbf{r}_{CS}) \sim W(y)\sqrt{2\pi/(k_0 r)}\, e^{-\mathrm{i}(k_0 r - \frac{\pi}{4})} \Phi^{\mathrm{sec}\pm}(\varphi) + \sum_{q=0}^{Q} \tilde{A}_q^{\pm} V_q(y) e^{\mp \mathrm{i}\beta_q x}, \quad \pm x > 0,\ r \to \infty \tag{6}$$

where $W(y) = 1$ if $y < L$ or $y > L + w$ and 0 otherwise, $\Phi^{\mathrm{sec}\pm}(\varphi)$ are the far-field angular patterns of the secondary fields in regions #2 and #0 (i.e., above and below the slab), while $\tilde{A}_q^{\pm}$ are the amplitudes of the guided waves propagating along the slab, β_q being the propagation constants and $V_q(y)$ the cross-sectional fields of these waves. The latter quantities are the eigenvalues and eigenfunctions of the slab-waveguide problem.

For analytical treatment of the fields in and out of the slab, which has infinite boundaries parallel to the x-axis, Fourier transform in x will be used. This technique allows to reduce the dimensionality of the problem and to satisfy the boundary conditions for all x. Thus, the primary CSP field is presented as a Fourier (also called Sommerfeld) integral

$$E^{\mathrm{pr}}(\mathbf{r}, \mathbf{r}_{CS}) = \frac{1}{4\pi} \int_{-\infty}^{+\infty} g_0^{-1} e^{-\mathrm{i}\lambda(x - x_{CS})} e^{\mp g_0 (y - y_{CS})} \mathrm{d}\lambda, \tag{7}$$

where $g_0(\lambda) = (\lambda^2 - k_0^2)^{1/2}$ and $|y| > b|\cos\beta|$. The integration path runs along the real axis of the proper sheet of the associated two-sheet Riemann surface, where $\mathrm{Re}[g_0(\lambda)] > 0$

or $\mathrm{Im}[g_0(\lambda)] > 0$. The above inequality provides convergence of (7) and entails that $L > b|\cos\beta|$, i.e., the CSP branch-cut cannot intersect or touch the slab interface (see Fig. 1). Such limitations are natural in all CSP beams scattering problems [14], [22]. Note that the CSP wave spectrum (7) contains both propagating (if $|\lambda| < k_0$) and evanescent waves (if $|\lambda| > k_0$).

Next, we present the secondary field as a Fourier integral

$$E^{\mathrm{sec}}(\mathbf{r}, \mathbf{r}_{CS}) = \frac{1}{4\pi}\int_{-\infty}^{+\infty} e^{-\mathrm{i}\lambda(x-x_{CS})}\gamma\,(\lambda, y; y_{CS})\,\mathrm{d}\lambda, \quad (8)$$

where the unknown function γ is found from the boundary conditions as (for $y \le L$, $L \le y \le L+w$, and $y \ge L+w$, respectively):

$$\gamma\,(\lambda, y, y_{CS}) = \begin{cases} A_1 \exp[g_0(\lambda)(y-L)] \\ A_2 \cosh\left[g_1(\lambda)\left(y-L-\dfrac{w}{2}\right)\right] \\ \quad +A_3 \sinh\left[g_1(\lambda)\left(y-L-\dfrac{w}{2}\right)\right] \\ A_4 \exp[-g_0(\lambda)(y-L-w)]. \end{cases} \quad (9)$$

The unknown coefficients $A_j = A_j(\lambda)$, $j = 1, \ldots, 4$ are determined explicitly by imposing the transmission boundary conditions at the interfaces $y = L$ and $y = L+w$, respectively, as follows:

$$A_1 = \frac{\left(g_0^2 - g_1^2\right)\sinh(g_1 w)}{\Delta^e(\lambda)\Delta^o(\lambda)}\frac{e^{-g_0(L-y_{CS})}}{2g_0}, \quad A_2 = \frac{e^{-g_0(L-y_{CS})}}{\Delta^e(\lambda)} \quad (10a)$$

$$A_3 = -\frac{e^{-g_0(L-y_{CS})}}{\Delta^o(\lambda)}, \quad A_4 = \frac{g_1\, e^{-g_0(L-y_{CS})}}{\Delta^e(\lambda)\Delta^o(\lambda)}. \quad (10b)$$

From (10), we see that the transcendental equation determining the poles of the integrand function γ in (8) is

$$\Delta(\lambda) = \Delta^e(\lambda)\Delta^o(\lambda) \quad (11)$$

where

$$\Delta^e(\lambda) = g_0(\lambda)\cosh\left[g_1(\lambda)\frac{w}{2}\right] + g_1(\lambda)\sinh\left[g_1(\lambda)\frac{w}{2}\right] = 0 \quad (12a)$$

$$\Delta^o(\lambda) = g_0(\lambda)\sinh\left[g_1(\lambda)\frac{w}{2}\right] + g_1(\lambda)\cosh\left[g_1(\lambda)\frac{w}{2}\right] = 0 \quad (12b)$$

with the indices e and o referring to the even and odd waves. The roots of $\Delta(\lambda)$, are denoted by $\lambda = \pm\beta_q$ ($q = 0, 1, 2, \ldots, Q$). Real-valued roots β_q are finite in number and located between k_0 and k_1 [35], [36]. The principal root ($q = 0$) exists at arbitrary frequency and slab contrast while the higher-order real roots ($q = 1, 2, \ldots$) appear if $k_0 w(\varepsilon_r - 1)^{1/2} \ge q\pi$. They are the propagation constants of the natural waves of the lossless dielectric-slab waveguide, with symmetric and antisymmetric field patterns with respect to the middle line of the slab, respectively.

III. Far-Field Patterns and Space-Wave Powers

The total electric field E^{tot} in the lower half-plane (region #0) determined by $y < -b|\cos\beta|$ is the sum of the CSP primary field, given by (7), and the secondary field, given by (8), (9), and (10a)

$$E^{\mathrm{sec}}(x, y; b, \beta) = \frac{1}{4\pi}\int_{-\infty}^{+\infty} e^{-\mathrm{i}\lambda(x+\mathrm{i}b\cos\beta)} \times \frac{e^{g_0 y}}{g_0}\frac{\left(g_0^2 - g_1^2\right)\sinh(g_1 w)}{2\Delta^e(\lambda)\Delta^o(\lambda)} e^{-g_0(\mathrm{i}b\sin\beta + 2L)}\,\mathrm{d}\lambda. \quad (13)$$

We will determine the total far-field angular pattern in the lower half-plane by employing the steepest descent method as follows. First, we apply transformation $\lambda = k_0\cos\xi$ to (13), and then introduce polar variables to get

$$E^{\mathrm{sec}}(r, \varphi; b, \beta) = \int_{C_\xi} \tilde{\delta}(\xi)\, e^{\rho\tilde{q}(\xi)}\,\mathrm{d}\xi, \quad \pi < \varphi < 2\pi \quad (14)$$

with C_ξ the integration contour in the complex ξ-domain, and

$$\tilde{\delta}(\xi) = \frac{\mathrm{i}}{4\pi}\frac{\left(k_1^2 - k_0^2\right)\sinh[g_1(k_0\cos\xi)w]}{2\Delta(k_0\cos\xi)} \times e^{k_0 b\cos(\xi-\beta)} e^{-2\mathrm{i}k_0 L\sin\xi} \quad (15a)$$

$$\tilde{q}(\xi) = -\mathrm{i}k_0\cos(\xi + \varphi). \quad (15b)$$

For $r \to \infty$, the main contribution in the integral (14) comes from the vicinity of the saddle point $\xi_s = -\varphi$, which satisfies $\tilde{q}'(\xi_s) = 0$ and $\tilde{q}''(\xi_s) = \mathrm{i}k_0 \ne 0$. The integration contour C_ξ is then deformed to the steepest descent contour, defined by $\cos(\mathrm{Re}\xi + \varphi)\cosh(\mathrm{Im}\xi) = 1$, which passes through $\xi_s = -\varphi$.

Now, by [35] and [37], we get from (14) that

$$E^{\mathrm{sec}}(r, \varphi; b, \beta) \sim -\sqrt{\frac{-2\pi}{r\tilde{q}''(\xi_s)}}\tilde{\delta}(\xi_s)e^{r\tilde{q}(\xi_s)}, \quad r \to \infty, \quad \pi < \varphi < 2\pi \quad (16)$$

which takes the form

$$E^{\mathrm{sec}}(r, \varphi; b, \beta) \sim \sqrt{2\pi/(k_0 r)}\, e^{-\mathrm{i}\left(k_0 r - \frac{\pi}{4}\right)}\Phi^{\mathrm{sec}-}(\varphi) \quad (17)$$

where

$$\Phi^{\mathrm{sec}-}(\varphi) = \frac{-\mathrm{i}}{4\pi}\left(k_1^2 - k_0^2\right)\frac{\sinh[g_1(k_0\cos\varphi)w]}{2\Delta\left(k_0\cos\varphi\right)} \times e^{k_0 b\cos(\varphi+\beta) + 2\mathrm{i}k_0 L\sin\varphi}. \quad (18)$$

The total far-field pattern in the lower half-plane (reflection zone) is obtained as $\Phi^{\mathrm{tot}-} = \Phi^{\mathrm{pr}} + \Phi^{\mathrm{sec}-}$ with the aid of (5).

By performing similar calculations for the field in the upper half-plane (transmission zone, defined by $y > L + w$), we get

$$E^{\mathrm{sec}}(r, \varphi; b, \beta) \sim \sqrt{2\pi/(k_0 r)}\, e^{-\mathrm{i}\left(k_0 r - \frac{\pi}{4}\right)}\,\Phi^{\mathrm{sec}+}(\varphi),\ r \to \infty, \quad 0 < \varphi < \pi \quad (19)$$

where

$$\Phi^{\mathrm{sec}+}(\varphi) = \frac{k_0}{4\pi}\frac{g_1(k_0\cos\varphi)}{\Delta(k_0\cos\varphi)}\sin\varphi\, e^{k_0 b\cos(\varphi-\beta) + \mathrm{i}k_0 w\sin\varphi} \quad (20)$$

is the total far-field pattern in the upper half-plane. Note that $\Phi^{\mathrm{tot}\pm}(0) = \Phi^{\mathrm{tot}\pm}(\pi) = 0$, which is consistent with the fact that along the slab, the power is carried only by the guided waves.

Next, we calculate the powers lost due to scattering in the upper and lower half planes. These powers are, respectively, defined as the electromagnetic far-field powers exiting two semicircles of large radius $r = R \to \infty$. By following similar analysis to that of [22], we get that the total radiated powers in the upper and lower half planes are

$$P^{\mathrm{rad}\pm} = \frac{1}{2\mathrm{i}\omega\mu_0} \lim_{r\to\infty} \left[r \int_0^{\pm\pi} E^{\mathrm{tot}}(r,\varphi) \frac{\partial (E^{\mathrm{tot}}(r,\varphi))^*}{\partial r} \,\mathrm{d}\varphi \right] \tag{21}$$

where * denotes complex conjugation. By combining the latter with (17), we obtain that these radiated powers are

$$P^{\mathrm{rad}\pm} = \frac{\pi}{k_0 Z_0} \int_0^{\pm\pi} |\Phi^{\mathrm{tot}\pm}(\varphi)|^2 \,\mathrm{d}\varphi \tag{22}$$

and the total power radiated off the lossless slab is given by

$$P^{\mathrm{rad}} = P^{\mathrm{rad}+} + P^{\mathrm{rad}-}. \tag{23}$$

The radiated powers need to be normalized by a reference quantity; such a role can be played by the power radiated by an isolated CSP in the free space, given by [22]

$$P^{\mathrm{pr}} = \frac{1}{8k_0 Z_0} I_0(2k_0 b) \tag{24}$$

where I_0 is the zero-order modified Bessel function.

IV. Fields and Powers of Guided Waves

The Fourier-integral expression of the secondary field in region #0 (i.e., for $y \le L$) is written, by (8), (9), and (10a) as:

$$E^{\mathrm{sec}}(x,y;x_{CS},y_{CS}) = \frac{1}{4\pi} \int_C u(\lambda) e^{g_0(\lambda)(y+y_{CS}-2L)} e^{-\mathrm{i}\lambda(x-x_{CS})} \,\mathrm{d}\lambda \tag{25}$$

where

$$u(\lambda) = \frac{\left[g_0^2(\lambda) - g_1^2(\lambda)\right] \sinh[g_1(\lambda) w]}{2 g_0(\lambda)\, \Delta(\lambda)}. \tag{26}$$

The integration path C is depicted in Fig. 2. The square root g_0 is defined (as mentioned above) as $\mathrm{Re}[g_0(\lambda)] > 0$ and $\mathrm{Im}[g_0(\lambda)] > 0$ by means of the branch cut selection shown in Fig. 2, so that the decaying and outgoing wave condition for $y \to \pm\infty$ is satisfied at any point of C [36], [37]. The points $\lambda = \pm k_0$ are the branch-points and are always associated with the infinite space or half-space wavenumber(s). The above-mentioned real-valued propagation constants β_q of the lossless slab are shown in Fig. 2. They are the poles of function $u(\lambda)$, given by (26); other poles are complex and located on the improper sheet of the corresponding Riemann surface.

Now, to calculate the integral in (25), we assume that the distance in x is large (i.e., take the limit as $x \to +\infty$) and employ Cauchy's residue Theorem. The integration contour is deformed in the lower half-plane so that the poles, determined by (11), are captured (see Fig. 2). In this way, we get

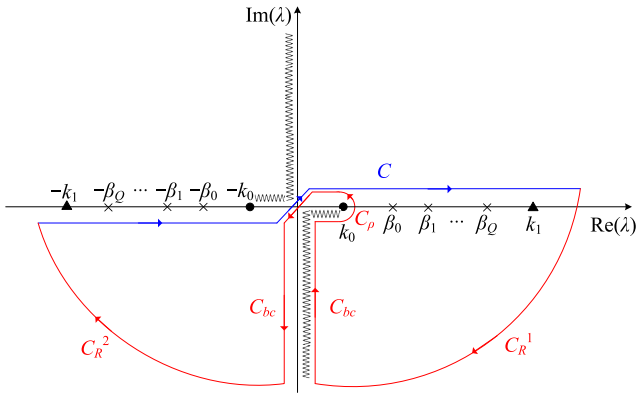

Fig. 2. Integration path C for the integral in (25), expressing the secondary (scattered) field in region #0. The contour deformation for the application of Cauchy's Theorem for $x > 0$ is also depicted.

$$\lim_{\substack{R\to\infty \\ \rho\to 0}} \left\{ \int_C + \int_{C_R^1 \cup C_R^2} + \int_{C_{bc}} + \int_{C_\rho} \right\} f(\lambda)\, d\lambda \to_{x\to+\infty} -2\pi\mathrm{i} \sum_{q=0}^{Q} \mathrm{Res}_{\lambda=\beta_q} f(\lambda), \tag{27}$$

$$f(\lambda) = \frac{1}{4\pi} u(\lambda) e^{g_0(\lambda)(y+y_{CS}-2L)} e^{-\mathrm{i}\lambda(x-x_{CS})}. \tag{28}$$

Indeed, it can be shown that the integral around the small circle C_ρ centered at the branch point $\lambda = +k_0$ tends to zero as the radius $\rho \to 0$. As noted in [8], [14], and [26], the integral along the branch cut C_{bc} is referred as the lateral wave. The main contribution to it is given by the integration in the vicinity of $\lambda = +k_0$ that can be expressed as asymptotic series of algebraically decreasing terms x^{-m}, $m = 1, 2, \ldots$ [23], [28]. Hence, the contribution of this integral vanishes as $x \to +\infty$. Moreover, the integrals along the two quarter-circles C_R^1 and C_R^2 vanish if $R \to \infty$ (it can be shown that $u(\lambda) \to 0$ as $R \to \infty$ and $\mathrm{Im}\ \lambda < 0$).

To this end, only the contribution of the residues at the guided-wave poles remains in (27). The residue at each pole produces the respective wave's field as follows:

$$\mathrm{Res}\left(f(\lambda), \lambda = \beta_q^{e,o}\right) = \frac{1}{8\pi} \left(g_0^2\left(\beta_q^{e,o}\right) - g_1^2\left(\beta_q^{e,o}\right)\right) \times \frac{\sinh\left[g_1\left(\beta_q^{e,o}\right) w\right] e^{g_0\left(\beta_q^{e,o}\right)(y+y_{CS}-2L)} e^{-\mathrm{i}\beta_q^{e,o}(x-x_{CS})}}{g_0\left(\beta_q^{e,o}\right) \Delta^{o,e}\left(\beta_q^{e,o}\right) \left.\frac{\mathrm{d}\Delta^{e,o}(\lambda)}{\mathrm{d}\lambda}\right|_{\lambda=\beta_q^{e,o}}} \tag{29}$$

where β_q^e and β_q^o denote, respectively, the propagation constants of the even and odd waves [i.e., the solutions of (12a) and (12b)]. Now, by (25), (27), and (29), and after lengthy calculations, we obtain

$$E^{\mathrm{sec}}(x,y;b,\beta) = \sum_{q=0}^{Q^e} A_{q,e}^{+} e^{g_0\left(\beta_q^e\right) y} e^{-\mathrm{i}\beta_q^e x} + \sum_{q=1}^{Q^o} A_{q,o}^{+} e^{g_0\left(\beta_q^o\right) y} e^{-\mathrm{i}\beta_q^o x} \tag{30}$$

where

$$A^{+}_{q,e} = \frac{\mathrm{i}\left(a_1\left(\beta^e_q\right)\right)^3 \tan\left(a_1\left(\beta^e_q\right)\frac{w}{2}\right)}{2\beta^e_q\left(k_0^2-k_1^2\right)\left(1+g_0\left(\beta^e_q\right)\frac{w}{2}\right)} \times e^{\beta^e_q b\cos\beta - g_0\left(\beta^e_q\right)(\mathrm{i}b\sin\beta+2L)} \tag{31a}$$

$$A^{+}_{q,o} = -\frac{\mathrm{i}\left[a_1\left(\beta^o_q\right)\right]^3 \cot\left(a_1\left(\beta^o_q\right)\frac{w}{2}\right)}{2\beta^o_q\left(k_0^2-k_1^2\right)\left(1+g_0\left(\beta^o_q\right)\frac{w}{2}\right)} \times e^{\beta^o_q b\cos\beta - g_0\left(\beta^o_q\right)(\mathrm{i}b\sin\beta+2L)}, \tag{31b}$$

are the amplitudes of the even and odd guided waves traveling along $+x$, while Q^e and Q^o denote, respectively, the total number of the even and odd eigenwaves (thus, $Q^e+Q^o=Q$). Also, we defined in (31) that $a_1(\lambda) = -\mathrm{i}g_1(\lambda) = -\mathrm{i}(k_0^2\varepsilon_r-\lambda^2)^{1/2}$.

Next, to calculate the integral in (25) for $x<0$, we close the integration path in the upper-half-plane. Then, by following the similar techniques as in the previous case of $x>0$, we obtain the final expression for $x\to-\infty$

$$E^{\mathrm{sec}}(x,y;b,\beta) = \sum_{q=0}^{Q^e} A^{-}_{q,e} e^{g_0\left(\beta^e_q\right)y} e^{\mathrm{i}\beta^e_q x} + \sum_{q=1}^{Q^o} A^{-}_{q,o} e^{g_0\left(\beta^o_q\right)y} e^{\mathrm{i}\beta^o_q x} \tag{32}$$

with the amplitudes of the even and odd guided waves traveling along the $-x$-direction, respectively, given by

$$A^{-}_{q,e} = \frac{\mathrm{i}\left(a_1\left(\beta^e_q\right)\right)^3 \tan\left(a_1\left(\beta^e_q\right)\frac{w}{2}\right)}{2\beta^e_q\left(k_0^2-k_1^2\right)\left(1+g_0\left(\beta^e_q\right)\frac{w}{2}\right)} \times e^{-\beta^e_q b\cos\beta - g_0\left(\beta^e_q\right)(\mathrm{i}b\sin\beta+2L)} \tag{33a}$$

$$A^{-}_{q,o} = -\frac{\mathrm{i}\left(a_1\left(\beta^o_q\right)\right)^3 \cot\left(a_1\left(\beta^o_q\right)\frac{w}{2}\right)}{2\beta^o_q\left(k_0^2-k_1^2\right)\left(1+g_0\left(\beta^o_q\right)\frac{w}{2}\right)} \times e^{-\beta^o_q b\cos\beta} e^{-g_0\left(\beta^o_q\right)(\mathrm{i}b\sin\beta+2L)}. \tag{33b}$$

Note that, as expected, for the normal incidence, i.e., for $\beta=\pi/2$, we have $A^{+}_{q,e}=A^{-}_{q,e}$ and $A^{+}_{q,o}=A^{-}_{q,o}$, that is the guided-wave powers split equally between the $+x$ and $-x$ directions.

The powers carried by the guided waves are then calculated from (30) and (32) by using the norms of the waves. More precisely, the even and odd eigenwaves are given by [29]

$$\Psi^e_q(x,y) = K_e e^{-\mathrm{i}\beta^e_q x} V^e_q(y) = K_e e^{-\mathrm{i}\beta^e_q x} \begin{cases} \cos\left(a_1\left(\beta^e_q\right)\frac{w}{2}\right) e^{-g_0\left(\beta^e_q\right)(y-(L+w))}, & y>L+w \\ \cos\left(a_1\left(\beta^e_q\right)\left(y-L-\frac{w}{2}\right)\right), & L<y<L+w \\ \cos\left(a_1\left(\beta^e_q\right)\frac{w}{2}\right) e^{g_0\left(\beta^e_q\right)(y-L)}, & y<L \end{cases} \tag{34a}$$

$$\Psi^o_q(x,y) = K_o e^{-\mathrm{i}\beta^o_q x} V^o_q(y) = K_o e^{-\mathrm{i}\beta^o_q x} \begin{cases} \sin\left(a_1\left(\beta^e_q\right)\frac{w}{2}\right) e^{-g_0\left(\beta^e_q\right)(y-(L+w))}, & y>L+w \\ \sin\left(a_1\left(\beta^e_q\right)\left(y-L-\frac{w}{2}\right)\right), & L<y<L+w \\ -\sin\left(a_1\left(\beta^e_q\right)\frac{w}{2}\right) e^{g_0\left(\beta^e_q\right)(y-L)}, & y<L \end{cases} \tag{34b}$$

where K_e and K_o are normalization parameters. With the help of [26, eq. (49)] and [27, eq. (7)], we get the norms of the guided waves, which can be used to normalize their powers as:

$$\left(N^e_q\right)^2 = \beta^e_q \int_{-\infty}^{+\infty} \left[V^e_q(y)\right]^2 \mathrm{d}y = \beta^e_q \left(\frac{\cos^2\left(a_1\left(\beta^e_q\right)\frac{w}{2}\right)}{g_0\left(\beta^e_q\right)} + \frac{\sin\left(2a_1\left(\beta^e_q\right)\frac{w}{2}\right)}{2a_1\left(\beta^e_q\right)} + \frac{w}{2}\right) \tag{35a}$$

$$\left(N^o_q\right)^2 = \beta^o_q \int_{-\infty}^{+\infty} \left[V^o_q(y)\right]^2 \mathrm{d}y = \beta^o_q \left(\frac{\sin^2\left(a_1\left(\beta^o_q\right)\frac{w}{2}\right)}{g_0\left(\beta^o_q\right)} - \frac{\sin\left(2a_1\left(\beta^o_q\right)\frac{w}{2}\right)}{2a_1\left(\beta^o_q\right)} + \frac{w}{2}\right). \tag{35b}$$

The powers of the guided waves traveling in the $+x$- and $-x$-directions are denoted by P^{gw+} and P^{gw-}, respectively. To calculate the latter guided-wave powers, we make the following considerations. By means of (30)–(34), we rewrite the secondary electric field's expressions $E^{\mathrm{sec}\pm}$ for waves traveling parallel to the $\pm x$-directions, respectively, as:

$$E^{\mathrm{sec}\pm}(x,y;b,\beta) = \sum_{q=0}^{Q^e} \tilde{A}^{\pm}_{q,e} V^e_q(y) e^{\mp\mathrm{i}\beta^e_q x} + \sum_{q=1}^{Q^o} \tilde{A}^{\pm}_{q,o} V^o_q(y) e^{\mp\mathrm{i}\beta^o_q x} \tag{36}$$

where

$$\tilde{A}^{\pm}_{q,e} = \frac{\mathrm{i}\left(a_1\left(\beta^e_q\right)\right)^3}{2\beta^e_q\left(k_0^2-k_1^2\right)\left(1+g_0\left(\beta^e_q\right)\frac{w}{2}\right)} \frac{\tan\left(a_1\left(\beta^e_q\right)\frac{w}{2}\right)}{\cos\left(a_1\left(\beta^e_q\right)\frac{w}{2}\right)} \times e^{\pm\beta^e_q b\cos\beta} e^{-g_0\left(\beta^e_q\right)(\mathrm{i}b\sin\beta+L)} \tag{37a}$$

$$\tilde{A}^{\pm}_{q,o} = \frac{\mathrm{i}\left(a_1\left(\beta^o_q\right)\right)^3}{2\beta^o_q\left(k_0^2-k_1^2\right)\left(1+g_0\left(\beta^o_q\right)\frac{w}{2}\right)} \frac{\cot\left(a_1\left(\beta^o_q\right)\frac{w}{2}\right)}{\sin\left(a_1\left(\beta^o_q\right)\frac{w}{2}\right)} \times e^{\pm\beta^o_q b\cos\beta} e^{-g_0\left(\beta^o_q\right)(\mathrm{i}b\sin\beta+L)}. \tag{37b}$$

Finally, by using (36), and considering [25, eq. (25)], [26, eq. (10)], and [27, eq. (7)], we get the expressions

$$P^{\mathrm{gw}\pm} = \frac{1}{2k_0 Z_0}\left(\sum_{q=0}^{Q^e}\left(N^e_q\right)^2\left|\tilde{A}^{\pm}_{q,e}\right|^2 + \sum_{q=1}^{Q^o}\left(N^o_q\right)^2\left|\tilde{A}^{\pm}_{q,o}\right|^2\right) \tag{38}$$

where $Z_0=(\mu_0/\varepsilon_0)^{1/2}$ is the free-space impedance.

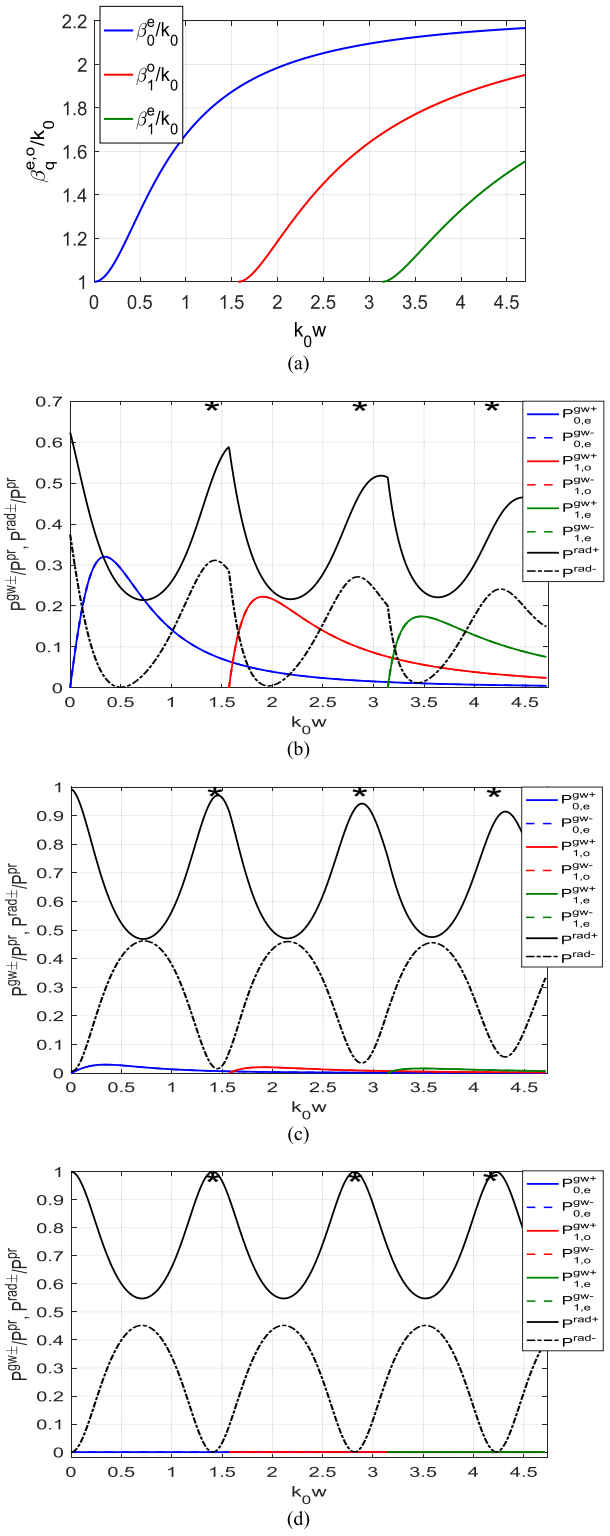

Fig. 3. (a) Dispersion curves of the first three guided waves of the dielectric slab TE$_q$, $q = 0, 1, 2$. (b)–(d) Normalized guided-waves powers $P^{\mathrm{gw}\pm}/P^{\mathrm{pr}}$ and space-wave powers $P^{\mathrm{rad}\pm}/P^{\mathrm{pr}}$ versus $k_0 w$ for $\varepsilon_r = 5$, $k_0 L = 0.21$ under the normal incidence of CSP beam, $\beta = 90°$ with (b) $k_0 b = 0.2$, (c) $k_0 b = 2$, and (d) $k_0 b = 20$.

Note that, in general, any CSP beam excites the guided waves in both directions along the slab, though their amplitudes can be very different (this is demonstrated for near-grazing incidence by the numerical results of the next section).

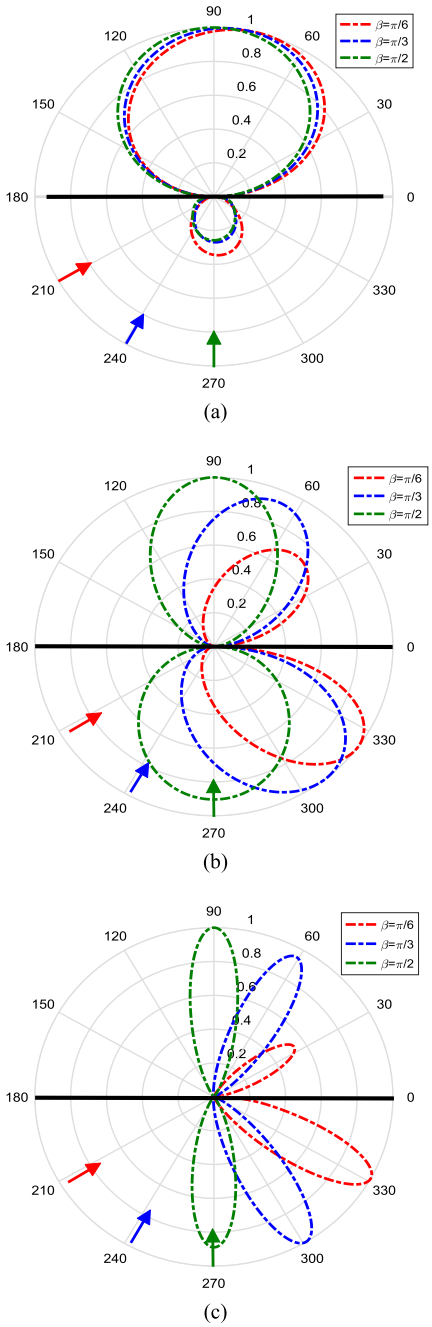

Fig. 4. Normalized total far-field patterns for a slab with $k_0 w = 0.75$, $\varepsilon_r = 5$, and CSP with parameters (a) $k_0 b = 0.2$, $k_0 L = 0.21$. (b) $k_0 b = 2$, $k_0 L = 2.1$. (c) $k_0 b = 20$, $k_0 L = 21$. For each case, three CSP orientation angles are considered: $\beta = \pi/6$, $\pi/3$, and $\pi/2$ as indicated by the corresponding arrows of the same color. The thick horizontal black line marks the presence of the slab. (a) Wide beam incidence. (b) Moderate beam incidence. (c) Narrow beam incidence.

V. Numerical Results and Discussion

To study the distribution of power fractions between the space waves and the guided waves, we have computed the dependences of these quantities on the electric thickness of the slab, i.e., the normalized frequency (Fig. 3). As known, the principal, even-type guided wave of the slab (TE$_0$) has no cutoff frequency, i.e., propagates along any finite-thickness slab, no matter how thin. However, if $k_0 w(\varepsilon_r - 1)^{1/2} = q\pi$, $q = 1, 2, \ldots$, then the higher-order guided waves (TE$_q$) start propagating as well [Fig. 3(a)]. These values are the

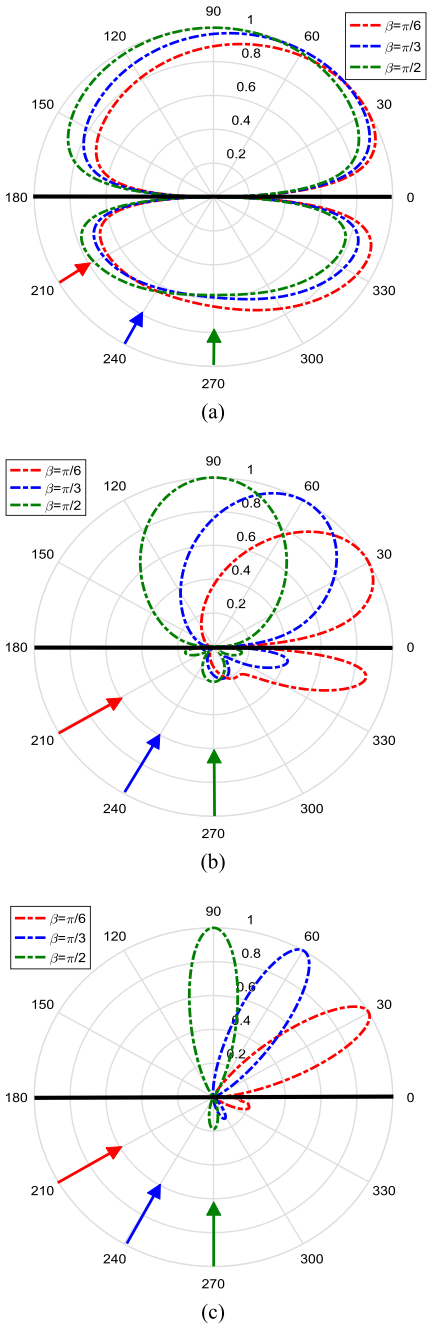

Fig. 5. Same as in Fig. 4, however, for $k_0 w = 1.5$. (a) Wide beam incidence. (b) Moderate beam incidence. (c) Narrow beam incidence.

branch points of the field as a function of the frequency. Therefore, the curves on the other panels display sharp bends at these frequencies, especially clearly visible on Fig. 3(b). These panels correspond to three different CSP beams: wide [Fig. 3(b)], moderate [Fig. 3(c)], and narrow [Fig. 3(d)]. Note that the transmitted space-wave powers $P^{\mathrm{rad}+}/P^{\mathrm{pr}}$ reach maxima at almost the same values of $k_0 w$ in all three cases. These values are very close to the natural frequencies of the slab as open dielectric cavity (marked with stars) [38]. Asymptotically, they are given by $(m = 0, 1, 2, \ldots)$

$$(k_0 w)_m = \pi (m+1)\varepsilon_r^{-1/2} + \mathrm{i}(1/2)\ln\left[\left(\varepsilon_r^{1/2}+1\right)/\left(\varepsilon_r^{1/2}-1\right)\right]. \tag{39}$$

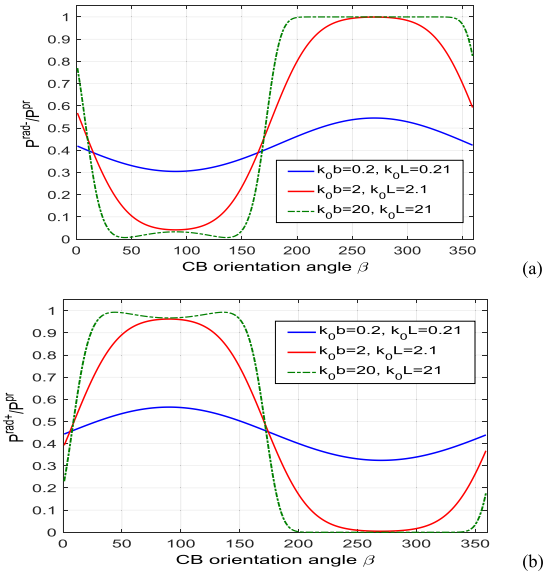

Fig. 6. Normalized radiated powers (a) $P^{\mathrm{rad}-}/P^{\mathrm{pr}}$ and (b) $P^{\mathrm{rad}+}/P^{\mathrm{pr}}$ versus the CSP beam incidence angle β, for $k_0 w = 1.5$, $\varepsilon_r = 5$, and $k_0 b = 0.2$, $k_0 L = 0.21$ (blue solid lines), $k_0 b = 2$, $k_0 L = 2.1$ (red dashed lines), and $k_0 b = 20$, $k_0 L = 21$ (green dashed-dotted lines).

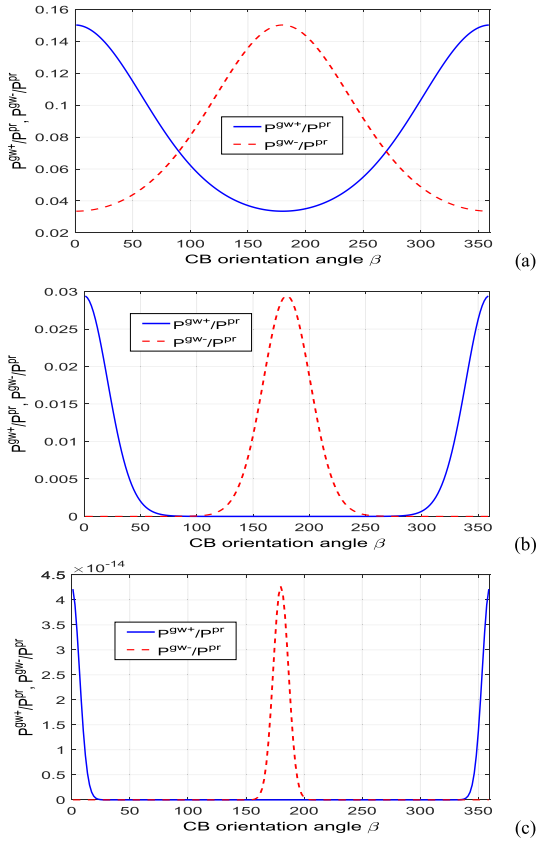

Fig. 7. Normalized guided-wave powers $P^{\mathrm{gw}\pm}/P^{\mathrm{pr}}$ [given by (38) and corresponding to waves traveling in the $\pm$ x-direction, respectively] as functions of the CSP beam orientation angle β for (a) $k_0 b = 0.2$, $k_0 L = 0.21$, (b) $k_0 b = 2$, $k_0 L = 2.1$, and (c) $k_0 b = 20$, $k_0 L = 21$, and a slab with $k_0 w = 1.5$, $\varepsilon_r = 5$.

At these resonant frequencies, the space-wave power below the slab, $P^{\mathrm{rad}-}$, exhibits extrema; either maxima for a wide beam [panel (b)] or minima for a narrow beam [panel (d)].

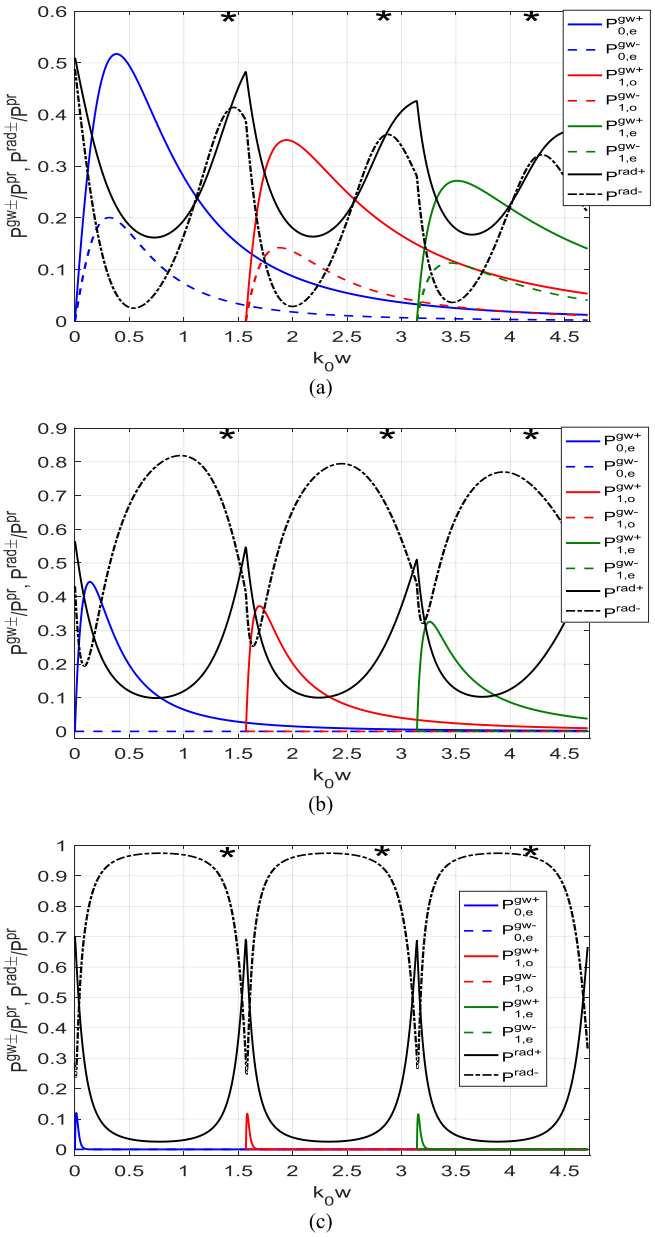

Fig. 8. Normalized guided-wave powers $P^{\mathrm{gw}\pm}/P^{\mathrm{pr}}$ and space-wave powers $P^{\mathrm{rad}\pm}/P^{\mathrm{pr}\pm}$ versus k_0w for the near-grazing CSP beam incidence at $\beta = 5°$, and (a) $k_0b = 0.2$ and $k_0L = 0.21$, (b) $k_0b = 2$ and $k_0L = 2.1$, and (c) $k_0b = 20$ and $k_0L = 21$, respectively.

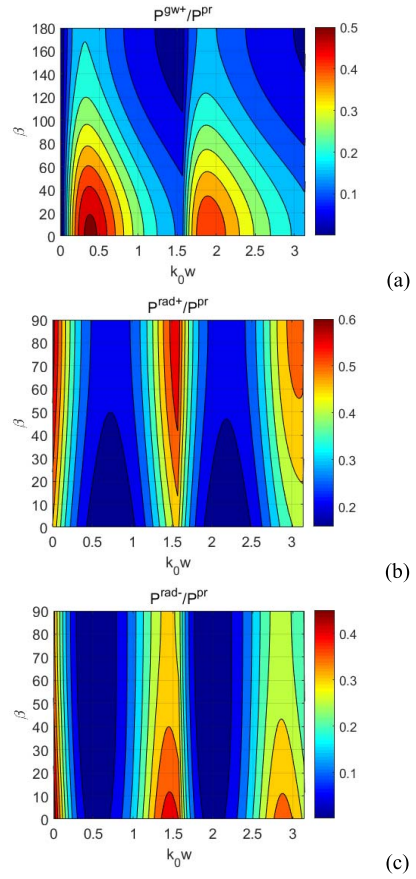

Fig. 9. Color maps of the normalized (a) guided-wave powers $P^{\mathrm{gw}+}/P^{\mathrm{pr}}$ and (b) and (c) space-wave powers $P^{\mathrm{rad}\pm}/P^{\mathrm{pr}}$ versus k_0w and β, for $k_0b = 0.2$ and $k_0L = 0.21$.

Additionally, unlike a wide beam, for the narrow beams the powers of the guided waves are very low. Thus, almost all the power goes through such a slab. Indeed, the frequencies of $k_0w = \pi(m+1)\varepsilon_r^{-1/2}$, $m = 0, 1, 2, \ldots$, are known as full transparency conditions for the lossless slab illuminated by the normally incident plane wave (see [39, Sec. IV-C]). Further, for the narrower beams [panels (c) and (d)], one can see the effect of the almost equal splitting of the space wave power between the transmission (upper) and the reflection (lower) half-spaces at $k_0w = \pi(1/2+m)\varepsilon_r^{-1/2}$, $m = 0, \ldots$ i.e., at *the quarter-wavelength in material* slab thickness.

Fig. 4 depicts the normalized total far-field patterns for a single-mode slab with $k_0w = 0.75$ and $\varepsilon_r = 5$, excited by three CSP beams with $\beta = \pi/2$, $\pi/3$, $\pi/6$, and distances from the CSP center to the slab $k_0L = 0.21, 2.1, 21$, respectively; thus $L > b|\cos\beta|$ and the aperture does not intersect or touch the slab.

Evidently, more directive CSP beams (i.e., with increasing k_0b), yield more directive far-field patterns. Besides, narrow CSP beams [panels (b) and (c)] show the mentioned power splitting as the selected thickness is quite near to the "quarter-wavelength in material" value. This effect, however, is degraded if the incidence deviates from normal, so that more power is reflected than transmitted. In contrast, if the thickness of the same slab is taken as $k_0w = 1.5$, as in Fig. 5, we see almost total transmission of the narrow beams [panels (b) and (c)]. This is because here the normalized frequency is close to the "half-wavelength in material" that is the same as the "full-transparency for the plane wave" condition, mentioned above. This effect also gets degraded if the beam incidence is inclined or if the beam becomes less narrow.

In Fig. 6, we depict the normalized total space-wave powers $P^{\mathrm{rad}-}/P^{\mathrm{pr}}$ and $P^{\mathrm{rad}+}/P^{\mathrm{pr}}$, versus the CSP orientation angle β for a slab with $k_0w = 1.5$ and $\varepsilon_r = 5$, and CSP apertures: 1) $k_0b = 0.2$, $k_0L = 0.21$; 2) $k_0b = 2$, $k_0L = 2.1$; and 3) $k_0b = 20$, $k_0L = 21$. As visible, if the CSP beam "looks at the slab," then the effect of nearly full transparency plays major role. The corresponding plots take shape of

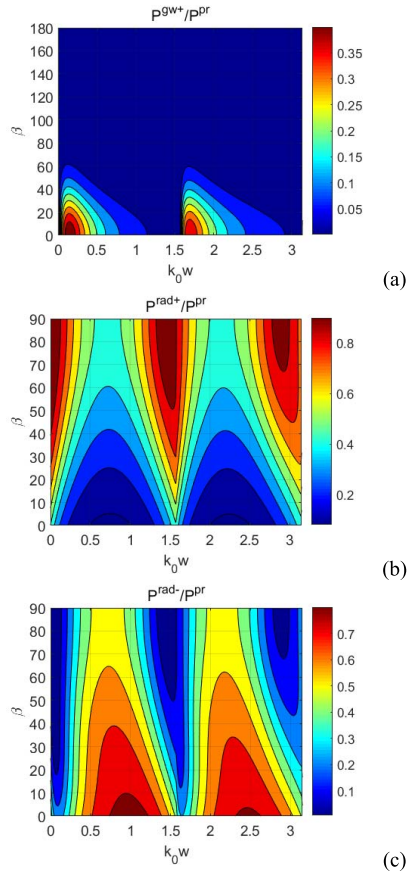

Fig. 10. Same as in Fig. 9, however, for $k_0b = 2$ and $k_0L = 2.1$.

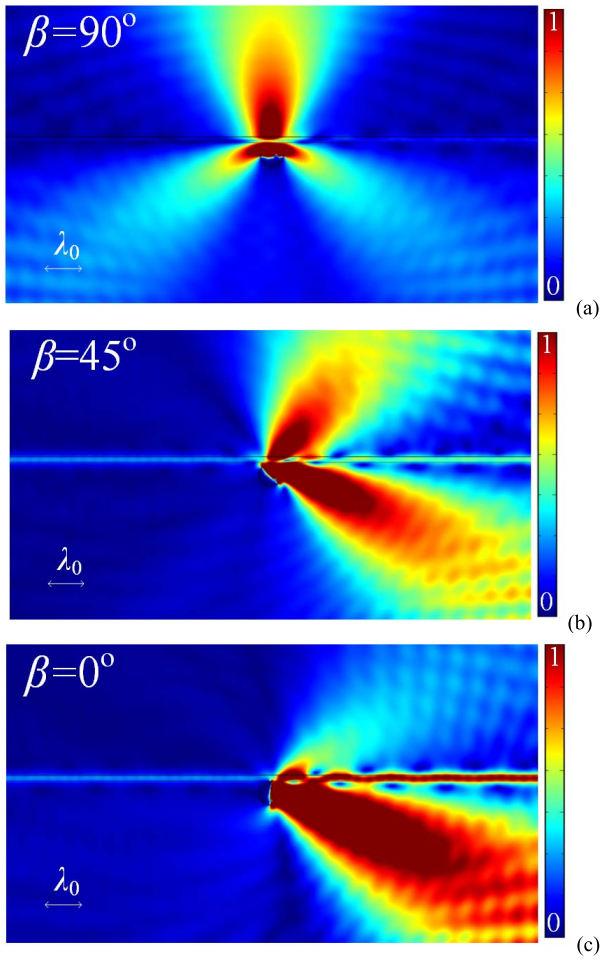

Fig. 11. Magnitude of the total electric field as computed by COMSOL for a dielectric slab with $k_0w = 1$, $\varepsilon_r = 5$ and a CSP beam with $k_0b = 2$, $k_0L = 2.1$ and (a) $\beta = 90°$, (b) $\beta = 45°$, and (c) $\beta = 0°$. The free-space wavelength λ_0 is also depicted.

two complementary unit step functions if the aperture gets larger and, thus, the beam gets more collimated.

Intuition suggests that the grazing incidence of the beam (i.e., $\beta = 0$ and π) is more favorable for the guided-waves excitation. To check this, in Fig. 7, we show the normalized guided-waves powers $P^{\mathrm{gw}+}/P^{\mathrm{pr}}$ and $P^{\mathrm{gw}-}/P^{\mathrm{pr}}$ versus the CSP angle β. The slab and beams are the same as in Fig. 6. Each of these curves has only one maximum either at $\beta = 0$ or $\beta = \pi$. Thus, the guided waves are indeed excited most efficiently if the CSP beam is in the grazing incidence; although the more collimated the beam the smaller the power of the guided wave. Note that at the grazing incidence, only one guided wave is excited with reasonable amplitude, traveling in the same direction where the beam is "looking," while the amplitude of the oppositely traveling wave remains far smaller.

To clarify the efficiency of the guided-wave excitation, we computed the associated power fractions versus the normalized frequency for the near-grazing incidence, $\beta = 5°$, of the same three CSP beams as before. These results are shown in Fig. 8. Together with Fig. 3, they convincingly reveal that the near-grazing beam incidence is accompanied by the launching of intensive guided waves of the slab each time the normalized frequency crosses the corresponding cutoff value. This is valid for the principal guided wave TE_0 that has zero cutoff frequency. At the same frequencies, the transmitted space-wave power reaches a maximum while the reflected power drops to a minimum and the narrower the beam, the sharper these effects and closer to the cutoff frequency.

To obtain a better insight into the revealed phenomena, we computed the color maps (i.e., reliefs) of the above normalized powers as function of two variables: the normalized frequency and the CSP beam incidence angle. They are presented in Figs. 9 and 10 for two beams, wide and moderately narrow, respectively. Note that the curves of Figs. 9(b) and (c) and 10(b) and (c) for the space-wave powers $P^{\mathrm{rad}\pm}/P^{\mathrm{pr}}$ are depicted for the CSP orientation angle β lying in $[0°, 90°]$ due to the obvious symmetry with respect to the normal incidence. Importantly, the maps of Figs. 9 and 10 support our main finding: the guided wave of the dielectric slab waveguide is efficiently excited by a CSP beam in the grazing illumination regime. Although this effect is degraded if the beam becomes more collimated, the guided waves can carry the power, which is comparable and even larger that the power of the space waves, i.e., reflected and transmitted beams. On the one hand, this effect can be used for designing surface-wave launchers. On the other hand, it should be taken into account, for instance, while designing the flat radomes of phased-array antennas where the guided waves should be eliminated.

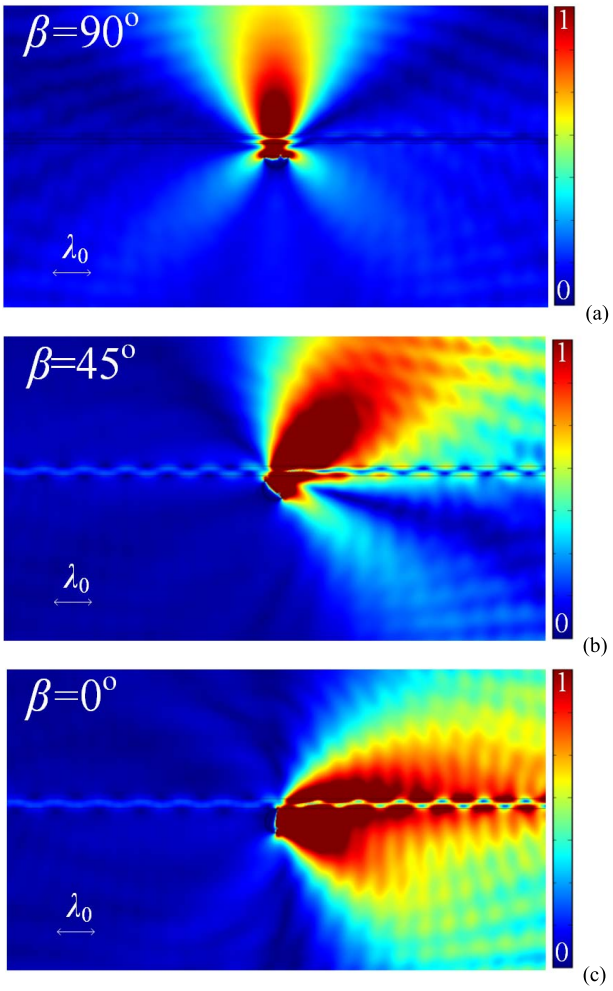

Fig. 12. Same as in Fig. 11, however, for $k_0 w = 1.6$.

VI. Validation

As evident, our full-wave analytical solution does not use any meshing of any computational domain and any other discretization of the problem. Therefore, it does not suffer from bad convergence and needs only a moderate desktop computer to produce the results with machine precision. In fact, these results can be viewed as reference data for the partial validation of commercial codes or less accurate numerical techniques and algorithms. As an example of such validation, we simulated with the aid of COMSOL Multiphysics [40] several slab-CSP configurations considered in the previous sections. COMSOL is a widely used commercial code based on discretization of the considered space, solution of wave equation in each domain of mesh, and enforcement of boundary conditions along neighboring domains, namely implementation of the finite element method (FEM). In this connection, our aim was to check the most interesting finding of the analytical treatment: is it true that a nearly grazing CSP beam is able (in sharp contrast to a plane wave) to efficiently excite the guided waves of a dielectric slab? We selected two values of the slab electric thickness, $k_0 w = 1$ for a single-wave slab and $k_0 w = 1.6$ for a two-wave slab, a moderately narrow CSP beam with $k_0 b = 2$, and three values of the beam orientation angle, $\beta = 90°, 45°$, and $0°$ (grazing incidence). Near fields computed with COMSOL, are shown in Figs. 11 and 12. As one directly observes, the normally incident CSP beam partially goes through the thinner slab and almost completely through the thicker slab. In addition, no guided waves appear on the slab in each case. This is in full agreement with the curves in Fig. 3(c) depicting the fractions of power radiated into the lower and upper half-spaces. If the CSP beam illuminates the same two slabs under $\beta = 45°$, then the emergence of one-side guided wave becomes clearly visible in the field patterns, namely the principal wave TE_0 on the thinner slab and the first higher-order wave TE_1 on the thicker slab. Finally, at grazing incidence ($\beta = 0°$) the guided-wave magnitude in each case becomes comparable to the space-wave values near the CSP. This is again in full agreement with our accurate findings presented in Fig. 10 for the same beam as in the COMSOL setting.

Thus, our main result is fully supported by commercial code simulations. The demonstrated good agreement can be interpreted as a validation of our work. From a different point of view, it can also be seen as a partial validation of COMSOL, which is a well-reputed code, though its accuracy is not generally accessible in principle.

VII. Conclusion

We have analytically solved the scattering problem of a CSP beam exciting a lossless dielectric slab. Numerical results on the variations of the guided-wave and space-wave powers versus the beam and slab parameters and the operating frequency have been presented, which reveal that the guided waves of the dielectric slab, neglected in earlier publications, can be efficiently excited by a CSP beam in the grazing and near-grazing regimes. This finding is fully supported by the visualization of the near-field patterns for the same configurations with help from COMSOL software. The solution of a similar problem with two different semiinfinite media above and below the lossless dielectric slab is of significant mathematical/physical interest due to the presence of two different branch points and constitutes a future work direction.

References

[1] M. Tanaka, K. Tanaka, and O. Fukumitsu, "Transmission and reflection of a Gaussian beam at oblique incidence on a dielectric slab," *J. Opt. Soc. Amer.*, vol. 67, no. 6, pp. 819–825, Jun. 1977.

[2] L. Arthur, A. Read, M. Wong, and G. E. Reesor, "Displacement of an electromagnetic beam upon reflection from a dielectic slab," *J. Opt. Soc. Amer.*, vol. 68, no. 3, pp. 319–322, Mar. 1978.

[3] R. P. Riesz and R. Simon, "Reflection of a Gaussian beam from a dielectric slab," *J. Opt. Soc. Amer. A*, vol. 2, no. 11, pp. 1809–1817, Nov. 1985.

[4] Q. Li and R. J. Vernon, "Theoretical and experimental investigation of Gaussian beam transmission and reflection by a dielectric slab at 110 GHz," *IEEE Trans. Antennas Propag.*, vol. 54, no. 11, pp. 3449–3457, Nov. 2006.

[5] I. Aramburu, M. Lujua, G. Madariaga, M. A. Illarramendi, and J. Zubia, "Effect of finite beam size on the spatial and spectral response of a Fabry–Pérot interferometer," *Proc. SPIE.*, vol. 10452, May 2017, Art. no. 104524E.

[6] G. A. Deschamps, "Gaussian beam as a bundle of complex rays," *Electron. Lett.*, vol. 7, no. 23, pp. 684–685, Nov. 1971.

[7] J. W. Ra, H. L. Bertoni, and L. B. Felsen, "Reflection and transmission of beams at a dielectric interface," *SIAM J. Appl. Math.*, vol. 24, no. 3, pp. 396–413, May 1973.

[8] L. B. Felsen, "Complex-source-point solutions of the field equations and their relation to the propagation and scattering of Gaussian beams," in *Proc. Symp. Math., Inst. Nazionale di Alta Matematica*, vol. 18, pp. 39–56, 1976.

[9] G. Suedan and E. Jull, "Two-dimensional beam diffraction by a half-plane and wide slit," *IEEE Trans. Antennas Propag.*, vol. 35, no. 9, pp. 1077–1083, 1987.

[10] G. A. Suedan and E. V. Jull, "Beam diffraction by planar and parabolic reflectors," *IEEE Trans. Antennas Propag.*, vol. 39, no. 4, pp. 521–527, Apr. 1991.

[11] T. Oguzer, A. Altintas, and A. I. Nosich, "Accurate simulation of reflector antennas by the complex source-dual series approach," *IEEE Trans. Antennas Propag.*, vol. 43, no. 8, pp. 793–801, Aug. 1995.

[12] V. B. Yurchenko, A. Altintas, and A. I. Nosich, "Numerical optimization of a cylindrical reflector-in-radome antenna system," *IEEE Trans. Antennas Propag.*, vol. 47, no. 4, pp. 668–673, Apr. 1999.

[13] S. V. Boriskina, A. I. Nosich, and A. Altintas, "Effect of the imperfect flat Earth on the vertically polarized radiation of a cylindrical reflector antenna," *IEEE Trans. Antennas Propag.*, vol. 48, no. 2, pp. 285–292, Feb. 2000.

[14] A. V. Boriskin and A. I. Nosich, "Whispering-gallery and Luneburg-lens effects in a beam-fed circularly layered dielectric cylinder," *IEEE Trans. Antennas Propag.*, vol. 50, no. 9, pp. 1245–1249, Sep. 2002.

[15] V. S. Bulygin, T. M. Benson, Y. V. Gandel, and A. I. Nosich, "Full-wave analysis and optimization of a TARA-Like shield-assisted paraboloidal reflector antenna using a Nystrom-type method," *IEEE Trans. Antennas Propag.*, vol. 61, no. 10, pp. 4981–4989, Oct. 2013.

[16] J. J. Maciel and L. B. Felsen, "Gaussian beam analysis of propagation from an extended plane aperture distribution through dielectric layers. II. Circular cylindrical layer," *IEEE Trans. Antennas Propag.*, vol. 38, no. 10, pp. 1618–1624, Oct. 1990.

[17] A. Boag and R. Mittra, "Complex multipole beam approach to electromagnetic scattering problems," *IEEE Trans. Antennas Propag.*, vol. 42, no. 3, pp. 356–372, Mar. 1994.

[18] K. Tap, P. H. Pathak, and R. J. Burkholder, "Exact complex source point beam expansions for electromagnetic fields," *IEEE Trans. Antennas Propag.*, vol. 59, no. 9, pp. 3379–3390, Sep. 2011.

[19] S. Skokic, M. Casaletti, S. Maci, and S. B. Sørensen, "Complex conical beams for aperture field representations," *IEEE Trans. Antennas Propag.*, vol. 59, no. 2, pp. 611–622, Feb. 2011.

[20] D. Gagnon, J. Dumont, and L. J. Dubé, "Beam shaping using genetically optimized two-dimensional photonic crystals," *J. Opt. Soc. Amer. A*, vol. 29, no. 12, pp. 2673–2678, Dec. 2012.

[21] M. Katsav, E. Heyman, and L. Klinkenbusch, "Beam diffraction by a wedge: Exact and complex ray solutions," *IEEE Trans. Antennas Propag.*, vol. 62, no. 7, pp. 3731–3740, Jul. 2014.

[22] N. L. Tsitsas, C. A. Valagiannopoulos, and A. I. Nosich, "Scattering and absorption of a complex source point beam by a grounded lossy dielectric slab with a superstrate," *J. Opt.*, vol. 16, no. 10, Sep. 2014, Art. no. 105712.

[23] N. K. Uzunoglu and J. G. Fikioris, "Scattering from an inhomogeneity inside a dielectric-slab waveguide," *J. Opt. Soc. Amer.*, vol. 72, no. 5, pp. 628–637, May 1982.

[24] A. S. Andrenko and A. I. Nosich, "H-scattering of thin-film modes from periodic gratings of finite extent," *Microw. Opt. Technol. Lett.*, vol. 5, no. 7, pp. 333–337, Jun. 1992.

[25] A. I. Nosich, "Radiation conditions, limiting absorption principle, and general relations in open waveguide scattering," *J. Electromagn. Waves Appl.*, vol. 8, no. 3, pp. 329–353, Jan. 1994.

[26] A. I. Nosich and A. S. Andrenko, "Scattering and mode conversion by a screen-like inhomogeneity inside a dielectric slab waveguide," *IEEE Trans. Microw. Theory Techniq.*, vol. 42, no. 2, pp. 298–307, Feb. 1994.

[27] S. V. Boriskina and A. I. Nosich, "Radiation and absorption losses of the whispering-gallery-mode dielectric resonators excited by a dielectric waveguide," *IEEE Trans. Microw. Theory Techn.*, vol. 47, no. 2, pp. 224–231, Feb. 1999.

[28] I. D. Chremmos and N. K. Uzunoglu, "Analysis of coupling between two slab waveguides in the presence of ring resonators," *J. Opt. Soc. Amer. A*, vol. 21, no. 2, pp. 267–279, Feb. 2004.

[29] I. D. Chremmos and N. K. Uzunoglu, "Transmission and radiation in a slab waveguide coupled to a whispering-gallery resonator: Volume-integral-equation analysis," *J. Opt. Soc. Amer. A, Opt. Image Sci.*, vol. 21, no. 5, pp. 839–846, May 2004.

[30] A. V. Maslov, V. N. Astratov, and M. I. Bakunov, "Resonant propulsion of a microparticle by a surface wave," *Phys. Rev. A, Gen. Phys.*, vol. 87, no. 5, May 2013, Art. no. 053848.

[31] A. V. Maslov, "Accurate computation of guided-wave coupling to dielectric resonators in 2-D geoetry," *IEEE Trans. Antennas Propag.*, vol. 66, no. 6, pp. 2904–2910, Jun. 2018.

[32] G. Ciraolo and R. Magnanini, "A radiation condition for uniqueness in a wave propagation problem for 2-D open waveguides," *Math. Meth. Appl. Sci.*, vol. 32, no. 10, pp. 1183–1206, Jul. 2009.

[33] O. P. Bruno and C. Pérez-Arancibia, "Windowed Green function method for the Helmholtz equation in the presence of multiply layered media," *Proc. Roy. Soc. A, Math., Phys. Eng. Sci.*, vol. 473, no. 2202, Jun. 2017, Art. no. 20170161.

[34] N. L. Tsitsas, "Complex source point beam excitation of a lossless dielectric slab," in *Proc. Int. Conf. Math. Methods Electromagn. Theory (MMET)*, Lviv, Ukraine, Jul. 2016, pp. 345–348.

[35] L. B. Felsen and N. Markuwitz, *Radiation and Scattering of Waves*. New York, NY, USA: Wiley, 2001, sec. 4.2a.

[36] E. J. Rothwell and M. J. Cloud, *Electromagnetics*. Boca Raton, FL, USA: CRC Press, 2018, sec. 5.6.

[37] R. E. Collin, *Field Theory of Guided Waves*. New York, NY, USA: McGraw-Hill, 1960.

[38] V. O. Byelobrov and A. I. Nosich, "Mathematical analysis of the lasing eigenvalue problem for the optical modes in a layered dielectric cavity with a quantum well and distributed Bragg reflectors," *Opt. Quant. Electron.*, vol. 39, nos. 10–11, pp. 927–937, Aug. 2007.

[39] O. V. Shapoval, R. Sauleau, and A. I. Nosich, "Scattering and absorption of waves by flat material strips analyzed using generalized boundary conditions and Nystrom-type algorithm," *IEEE Trans. Antennas Propag.*, vol. 59, no. 9, pp. 3339–3346, Sep. 2011.

[40] *Comsol Multiphysics Modeling Software*. Accessed: Feb. 10, 2019. [Online]. Available: https://www.comsol.com/

Nikolaos L. Tsitsas (S'03–M'06) was born in Athens, Greece, in 1979. He received the Diploma degree in electrical engineering from the National Technical University of Athens (NTUA), Athens, in 2002, the M.Sc. degree in applied mathematics from the National and Kapodistrian University of Athens, Athens, in 2005, and the Ph.D. degree in computational electromagnetics from NTUA in 2006.

From 2008 to 2011, he was an Adjunct Lecturer with the School of Applied Mathematical and Physical Sciences, NTUA. From 2009 to 2011, he was an Adjunct Lecturer with the Hellenic Army Academy, Vari, Greece. Since 2012, he has been an Assistant Professor with the School of Informatics, Aristotle University of Thessaloniki, Thessaloniki, Greece. He has authored or coauthored 54 papers in scientific journals and more than 60 papers in conference proceedings. His current research interests include methodologies of applied mathematics in direct and inverse wave scattering and propagation theory.

Dr. Tsitsas is a member of the American Mathematical Society and the Technical Chamber of Greece and a Senior Member of the Optical Society of America.

Constantinos Valagiannopoulos (M'12–SM'16) was born in Athens, Greece, in 1982. He received the Dipl.-Eng. (Hons.) degree in electrical engineering and the Ph.D. degree in electromagnetic theory from the National Technical University of Athens, Athens, in 2004 and 2009, respectively.

From 2010 to 2014, he was a Post-Doctoral Researcher with the Group of Theoretical and Applied Electromagnetics of Complex Media, Department of Electronics and Nanoengineering, Aalto University, Espoo, Finland, under the supervision of S. Tretyakov. From 2014 to 2015, he was with the Laboratory of Metamaterials and Plasmonics, Department of Electrical and Computer Engineering, University of Texas at Austin, Austin, TX, USA, under the supervision of A. Alu. Since 2015, he has been an Assistant Professor with Nazarbayev University (NU), Astana, Kazakhstan, where he has also been an Associate Professor with the Department of Physics since 2018. He leads the Metamaterials Modeling and Design Group, NU, performing research on the forward and inverse design of photonic devices manipulating the light. He is currently participating as a Principal Investigator (PI) or co-PI in the successful execution of national and international winning research grants with total annual budget more than 450K USD. He has authored or coauthored more than 90 works published at international refereed scientific journals and presented numerous reports in scientific conferences.

Dr. Valagiannopoulos is currently a Senior Member of OSA. He was a recipient of the International Chorafas Prize for the Best Doctoral Thesis in 2008, the Academy of Finland Postdoctoral Grant from 2012 to 2015, and the inaugural 2015 JOPT Research Excellence Award for his work: "Perfect absorption in graphene multilayers."

Alexander I. Nosich (M'94–SM'95–F'04) was born in Kharkiv, Ukraine, in 1953. He received the M.S., Ph.D., and D.Sc. degrees in radio physics from Kharkiv National University, Kharkiv, in 1975, 1979, and 1990, respectively.

Since 1979, he has been with the Institute of Radio Physics and Electronics, National Academy of Sciences of Ukraine (NASU), Kharkiv, where he is currently a Professor, a Principal Scientist, and the Head of the Laboratory of Micro and Nano Optics. Since 1992, he has held many guest fellowships and professorships in the EU, U.K., Japan, Singapore, and Turkey. His current research interests include the method of analytical regularization, propagation, and scattering of waves, open waveguides, antennas and lasers, and the history of microwaves.

Professor Nosich was a co-recipient of the 2017 National Prize of Ukraine in Science and Technology for the works Photonics of Semiconductor and Dielectric Nanostructures and the 2018 S. I. Pekar Award of the National Academy of Sciences of Ukraine for the contributions to the solid-state physics theory. He received the honorary title of Doctor Honoris Causa from the University of Rennes 1, France, in 2015, and the Galileo Galilei Medal of the International Commission for Optics in 2017. He has been the Initiator and the Technical Committee Chairman of the International Conference Series on Mathematical Methods in Electromagnetic Theory (MMET), Ukraine, since 1990. In 1995, he organized the IEEE AP-S East Ukraine Chapter, the first one in the former USSR. He currently represents Ukraine in the European Association on Antennas and Propagation.